Using Direct and Indirect Methods to Assess the Influence of High-Energy Waves over Beach Sedimentary Balance (Brazilian Northeastern Region)

Authors: Eduardo, Letícia Mesquita, de Carvalho, Alexandre Medeiros, Lima Júnior, Sérgio Bezerra, Claudino-Sales, Vanda, da Costa Gastão, Francisco Gleidson, et al.

Source: Journal of Coastal Research, 37(6) : 1235-1246

Published By: Coastal Education and Research Foundation

URL: https://doi.org/10.2112/JCOASTRES-D-21-00024.1

Journal of Coastal Research	37	6	1235–1246	Coconut Creek, Florida	November 2021

Using Direct and Indirect Methods to Assess the Influence of High-Energy Waves over Beach Sedimentary Balance (Brazilian Northeastern Region)

www.cerf-jcr.org

Letícia Mesquita Eduardo[†], Alexandre Medeiros de Carvalho[†], Sérgio Bezerra Lima Júnior[†], Vanda Claudino-Sales[‡]*, Francisco Gleidson da Costa Gastão[†], Jonathan L. Castelo Branco[†], and Lidriana de Souza Pinheiro[†]

[†]Marine Sciences Institute (LABOMAR)
Federal University of Ceará, UFC, Brazil

[‡]Department of Geography
Federal University of Ceará, UFC, Brazil

www.JCRonline.org

ABSTRACT

Eduardo, L.M.; Carvalho, A.M.; Lima, S.B.; Claudino-Sales, V.; Costa Gastão, F.G.; Castelo Branco, J.L., and Souza Pinheiro, L., 2021. Using direct and indirect methods to assess the influence of high-energy waves over beach sedimentary balance (Brazilian Northeastern region). *Journal of Coastal Research,* 37(6), 1235–1246. Coconut Creek (Florida), ISSN 0749-0208.

Because of the high dynamicity of atmospheric and oceanographic variables in coastal processes, local sedimentary balance is a matter of great interest for Integrated Coastal Zone Management. The diversity of environmental factors associated with the history of anthropic interventions, in addition to detailed topographic changes related to storm surge events, is assessed in this research for a stretch of the northeastern Brazilian coast. For this purpose, an association of conventional and improved digital methods was applied for data acquisition and processing. Remote sensing techniques with unmanned aerial vehicles (UAVs), three-dimensional modeling, and sedimentary analysis were performed, as well as detailed monitoring of meteorological and oceanographic variables with *in situ* sources and environmental modeling. The results of 1-year monitoring revealed a sedimentary balance with different variations in response to high-energy events associated with extratropical cyclones in the North Atlantic. The sedimentary balance showed an erosional rate of 25.5%, reflected in a 17.4% diminution in average topographic level of the area. Beach erosion was correlated to long period waves and great variability of wave types. Positive volumetric changes were correlated to mild weather environmental conditions. Swell waves presented a significant role in both beach erosion and following consequential topographic recovery. There was an asymmetric susceptibility to volume losses in different beach sectors.

ADDITIONAL INDEX WORDS: Storm surge, sedimentary balance, coastal management, UAV.

INTRODUCTION

The interhemispheric dynamic that controls Southern Hemisphere high-energy waves incidence, in response to the formation of synoptic scale atmospheric systems in the Northern Hemisphere, has been continually documented around the world (Alves, 2006; Chen *et al*., 2002; Hamilton, 1992; Innocentini *et al*., 2000; Semedo *et al*., 2011; Vassie, Woodworth, and Holt, 2004) and, especially, in the Northeastern Brazilian coast (NEB) (Farias, 2012; Silva *et al*., 2011; Vianna, 2000).

Long period wave generation occurs in response to wind speeds greater than 18 m s^{-1} over areas of approximately 1000 km (Munk *et al*., 1963). This wind and fetch area pattern are usually associated with low-pressure storm centers, where swell waves originate (Barrer and Ursell, 1948). From this point on, swell waves propagate across the ocean with low dissipation coefficient (Drennan *et al*., 2003), dispersing throughout long distances on a global scale (Munk *et al*., 1963).

Details concerning the origin, occurrence pattern, and morphodynamic impacts of swell waves are of great interest for Integrated Coastal Zone Management (ICZM) (Casella *et al*., 2014; Guerra, 2014). Intense swell activity is particularly important in coastal dynamics when it coincides with maximum periods of spring tide, resulting in storm surge events. The evaluation of these factors in coastal areas faces challenges as the process of nearshore urbanization increases, where anthropic intervention background is already significant. On the Northeastern Brazilian coast, storm surges are frequently associated with the destruction over coastal protection and urbanization structures (Paula *et al*., 2015a).

Low-pressure cyclonic systems are frequent over the North Atlantic Ocean, particularly from January to July, when the region becomes one of the primary cyclogenesis zones (Mendes and Mendes, 2004; Trigo, Davies, and Bigg, 1999). The formation of such atmospheric systems, especially between 35°N and 65°N latitudes, generates swell wave packets that arrive at Ceará coast, in Northeast Brazil, with an average response time of 3 days (Farias, 2012).

Local storm surge events are characterized by the incidence of waves up to 2.8 m of significant height (*Hs*), peak periods (*T*) of 11.2 to 20 seconds, and NW to NE peak direction (*Dp*), which, when added to spring tide maximums, can reach resultant heights (*Hr*) up to 5 m (Fisch, 2008). The high energy associated with these events provides them with the capacity for rapid and intense changing of coastal landscape, through insertion or removal of sediments in different sectors of beach topography.

DOI: 10.2112/JCOASTRES-D-21-00024.1 received 18 February 2021; accepted in revision 15 May 2021; corrected proofs received 24 June 2021; published pre-print online 21 July 2021.
*Corresponding author: vcs@ufc.br

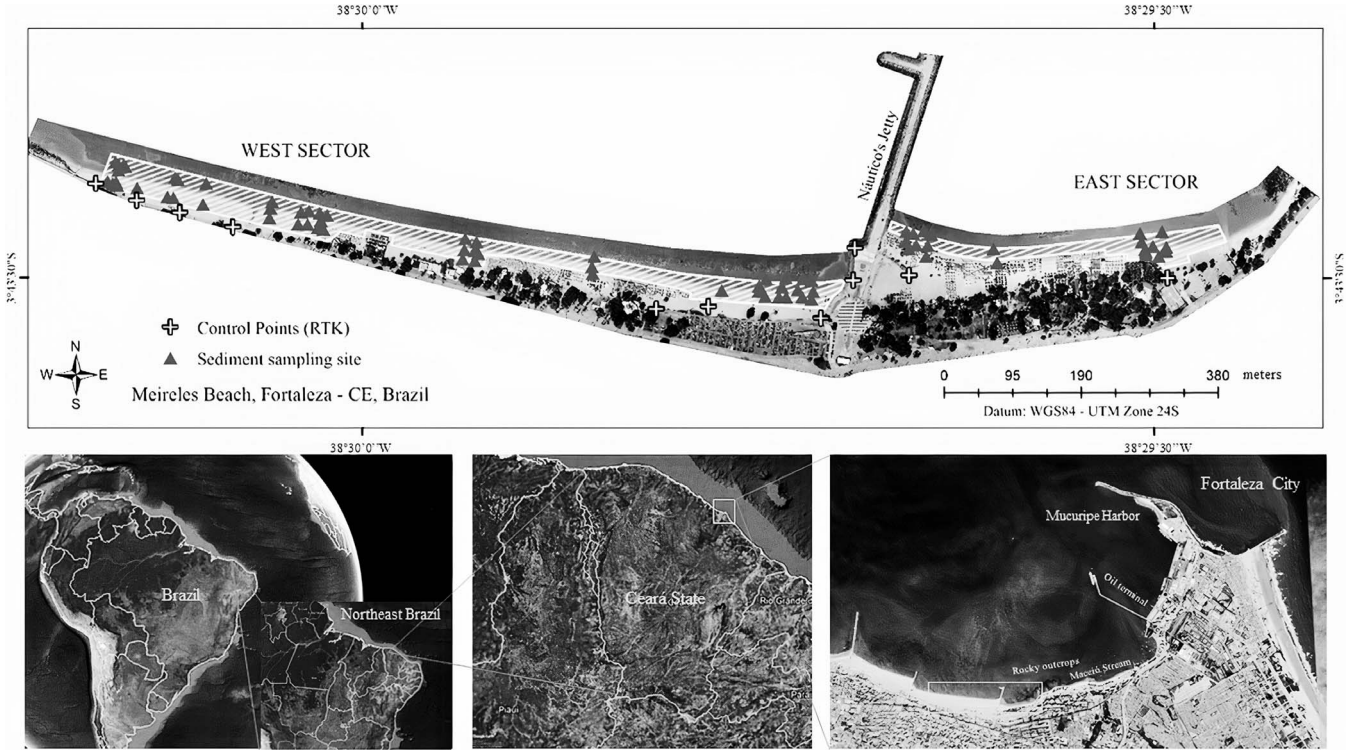

Figure 1. Location maps of the study site, showing (a) the survey area and its (b) global, (c) regional, and (d) local context. Figure 1a also shows the location of standardized polygons, RTK control points and sediment sampling sites. Figure 1d highlights important morphodynamic features, such as rocky Barreiras Formation outcrops, Maceió Stream, and port structures. Geographic coordinate system: Universal Transverse of Mercator (UTM); Datum: WGS84/Zone 24S.

In light of this highly dynamic scenario, an effective strategy, given by the association of direct and indirect methods, was required to match both the spatial and temporal scale necessary to show rapid and medium-term changes in coastal sedimentary balance. To address this, a broad assessment of environmental variables is proposed in response to cyclonic events in the North Atlantic, related to the topographic changes on the emerged sector of a coastal stretch in the Brazilian semiarid region.

Study Area

The study area is situated in the Brazilian northeastern region and is characterized in the following paragraphs:

General Location

The Brazilian northeastern region is composed of nine coastal states, with a coastline extension of nearly 3400 km and great geomorphologic variety (Pinheiro *et al*., 2008; Pinheiro, Morais, and Maia, 2016). Ceará State, located between intertropical latitudes of 2.5°S and 8°S and 37°W to 42°W longitudes, is in a tropical semiarid climate domain (Köppen, 1936) and has nearly 573 km of coastline extension. Fortaleza City, the state capital with nearly 2.7 million inhabitants (IPECE, 2018), exhibits a remarkably urbanized and anthropically modified coastline (Fechine, 2007).

The study site represents a 1 km portion (Figure 1a) from Fortaleza's 80 km coastline, which is characterized, according to Maia (1998), as a current sandy coastal system with punctual manifestation of Tertiary/Quaternary Barreiras Formation lithified deposits. Abrasion platforms develop over these deposits, eventually allowing beachrock formation. It is a coastal landscape historically artificialized by protection and recovery interventions, such as jetties and beach nourishment (Figure 1a,d).

Climatology and Environmental Variables

Fortaleza city's coastline is under the influence of a sub-humid tropical climate in which two distinct periods are identified: a rainy season (January–May) and a dry season throughout the rest of the year. Pluviometry rates, which in the rainy seasons concentrate up to 90% of the total, can reach nearly 1,400 mm/y, associated with a mean temperature of 27°C with low variation amplitude (IPECE, 2018).

Wind regime varies seasonally in an inversely proportional relation to rainfall pattern (Carvalho, 2003; Claudino-Sales, 1993; Claudino-Sales, Wang, and Carvalho, 2018), reaching minimum speed values in the first semester (2.0 m/s, average) and maximum values in the second half of the year (4.0 m/s, average). Wind directions are predominantly of E and ESE quadrants, under the primary influence of southeasterly trade winds (Chung, 1982; Utida *et al*., 2019).

The tidal regime is characterized by a semidiurnal and mesotidal system, subjected to a tidal variation range of 2 to 3 m—on neap tide and spring tide, respectively. Astronomic tides can reach maximum value of 3 m and minimum of –0.2 m.

Table 1. *Labels, dates, associated tide height, number of images and number of sedimentary samples collected in each mission.*

Labels	C1	C2	C3	C4	C5	C6	C7
Date	17 Apr 2018	18 May 2018	27 Jul 2018	26 Sep 2018	26 Nov 2018	23 Jan 2019	20 Mar 2019
Tide (m)	0.1	0.1	0.4	0.3	0.4	0.1	0.0
Number of images	194	192	198	247	204	191	255
Number of sediment samples	—	—	19	18	16	12	13

Ceará State's coast, as described by Fisch (2008), has essentially the four most common sea states. These are: (1) sea state associated with local winds, with maximum waves heights (Hs_{max}) of 1.1 m ($T(s) = 2$ to 5s, Dp = NW to E/SE); (2) sea state associated with northeasterly trade winds, with waves of $Hs_{max} = 1.1$ m ($T(s) = 8$ to 11, Dp = N to NE); (3) sea state associated with southeasterly trade winds, with $Hs_{max} = 2$ m ($T(s) = 5$ to 11, Dp = E to SE); and, finally, (4) dispersive arrivals from the northern hemisphere (NH), with $Hs_{max} = 2.8$ m ($T(s) = 11$ to 20, Dp = NW to NE).

Still, according to the observations of Fisch (2008), the dispersive arrival state is more frequently identified between January and March. Under the influence of southeast trade winds, sea states of greater energy can occur between September and November—when the withdrawal of the intertropical convergence zone (ITCZ) from the area allows the development of more intense winds.

Coastal Morphodynamic and History of Interventions

According to Maia (1998), the longshore sediment transport by wave action and wind are the most important processes for balance and evolution of Fortaleza's coastline. In this region, local morphodynamic aspects, as well as the interaction of multiple natural variables, were heavily affected by human interventions—expressed by preexistent and ongoing harboring structures, jetties, piers, beach nourishment projects, and coastline artificialization for urbanistic purposes (Fechine, 2007; Morais *et al*., 2018; Paula *et al*., 2015b). In this scenario, the Mucuripe Harbor (Figure 1d), since its construction, has acted as the most important feature of general impact on Fortaleza's coastline. As a result of its construction on the Mucuripe Headland without a detailed consideration of local hydrodynamic aspects, the structure promoted relevant impacts on wave propagation and sediment transportation patterns (Bezerra, Pinheiro, and Morais, 2007; Maia *et al*., 1996, 1998; Morais, 1980, 1981). The harbor's jetty construction interrupted the headland bypass process with sediments coming from east to west, propelling an erosive tendency along the coastline west to the structure.

From photographic historical records, before and during the port construction in the 1950s, the downstream Mucuripe promontory used to receive aeolian sediments from the updrift sector, which were directly deposited on the inside portion of the harbor, until being blocked after harbor construction. In response to the successive jetty installation and consequent retention of sediments transported by longshore current—always resulting in down-current erosion processes—effects of anthropic intervention extended beyond the limits of Fortaleza's western coast, remodeling the coastal landscape of Fortaleza itself and adjacent municipalities (Maia *et al*., 1998; Moura, 2012).

A close analysis of the survey area shows that Náutico's Jetty (Figure 1a) represents the most important artificial structure to be considered on wave incidence and sediment deposition dynamics. Secondarily, the presence of culverts and punctual areas of rocky outcrops is highlighted (Figure 1d). Updrift of the study site shows where the Maceió Stream (Figure 1d) is located, which was related to a contribution of fine granulometry sediments into the internal platform with an estimated flow rate of 0.02 m^3/s (Lima Filho, Castelo Branco, and Pinheiro, 2019).

METHODS

An ensemble of different methods were used in order to conduct the research:

Photogrammetry

The acquisition of aerial images was performed by the alternate application of two unmanned aerial vehicle (UAV) models: Phantom 4 (DJI Technology Co), associated with a DJI FC330 camera, as well as a Phantom 4 Advanced with an FC6310 camera. A flight plan was previously designed with DroneDeploy v.2.7.6.0, which guided the survey over an area of 48,700 m^2.

Monitoring the periodicity of activities followed bimonthly intervals from April 2018 to March 2019, resulting in seven flight missions—specified in Table 1.

Immediately before flight missions, the delimitation phase of Control Point (CP) was executed. The exact geographic location was obtained through a Geodesic GPS system with real time kinematic (RTK), using a Trimble R10 GNSS equipment. After in situ data acquisition, CPs were adjusted to ellipsoidal height and corrected by triangulation based on information gathered by two altimetric stations of the Brazilian network of continuous monitoring (RBMC). Finally, using MAPGEO 2015 (Brazilian Institute of Geography and Statistics—IBGE) software, altitude and geoid undulation verification and geometric to orthometric data corrections were executed. Aerial imagery was processed using OpenDroneMap v.0.4 for the final generation of digital elevation models (DEMs). A final report from OpenDroneMap provided the errors related to the delimitation of control points during DEM generation, which are shown in Table 2.

Comparative Analysis

In order to establish an equitable criterion of data analysis for all models, two standardized polygons were set for eastern and western sectors, taking as reference their positioning in relation to Náutico's rocky jetty. Fixing area and perimeter proportions made it possible to compare DEMs regardless of

Table 2. *Errors related to control points (CPs) delimitation during DEM generation, per survey and mean values.*

	Error (m)	Error (pix)	Z error (m)
C1	0.04336	0.630	0.00925
C2	0.04339	0.418	0.00561
C3	0.04109	0.279	0.01959
C4	0.03912	0.339	0.01015
C5	0.03076	0.429	0.00135
C6	0.04303	0.393	0.00362
C7	0.03532	0.270	0.00745
Mean error	0.03943	0.394	0.00814

limitations due to reflectance on the intertidal zone and allowed a more detailed visualization over areas under special morphodynamic circumstances. The standard polygon for the east sector covered an area of 6791 m^2 and 858 m perimeter, while the west sector covered 21,265 m^2 and 1855 m (Figure 2). Consequently, the east sector was expected to have smaller relative volumetric rates when compared to the west sector.

Quantitative comparisons between models involved the volume above custom level and mean level parameters, provided with calculations made by the software itself in DEM processing. The first one provides total volume measures in cubic meters over a suitable altimetric value, while the second describes the average altimetric level for the defined area.

Sedimentological Characterization

Throughout the aerial scanning missions, sedimentary sample collection occurred based on topographic and textural discrepancies visually identified among foreshore and backshore zones, but considering the same zone around the sampling point. A mean value of 18 samples per mission was gathered from July 2018 to March 2019, resulting in 78 sampling points (Figure 1).

Granulometric analysis followed the routine in Suguio (1973), using Wentworth's Sedimentary Scale (Wentworth, 1922) as reference. Dimensional, faciologic, and degree of selection were determined with Folk and Ward's classification (Folk and Ward, 1957). Grain size data were processed using SysGran v.3.1 software (Camargo, 2006).

Meteorological and Oceanographic Factors

The majority of oceanographic data was obtained using the WaveWatch III model application. Fortaleza's buoy data, from the National Buoy Program (PNBOIA, 2021), and official warnings from the Brazilian Navy were used as complementary information. Tide records were acquired through the platform of the Hydrography and Navigation Board (DNH, 2021).

A characterization of cyclonic systems in the NH, associated with the monitoring of the arrival of dispersive waves, was made with the National Oceanic and Atmospheric Administration (NOAA) Global Forecast System (GFS, 2020). Meteorological data, such as daily precipitation rates, wind speed, and direction were obtained from an *in situ* sensor from Fortaleza's Meteorological Station, monitored by the National Institute of Meteorology (INMET, 2020).

Environmental variables analysis was performed based on a monthly mean classification for the period available on WaveWatch III model database (2016 to 2020) and a daily classification for the surveyed period. For wave climate description, the classification of Fisch (2008) was applied to identify the arrival of dispersive swell waves from the northern hemisphere. Wave typology was conventionally made considering wave period, whether it was below (sea waves) or above (swell waves) 10 seconds. The characterization of high-energy events was based in not only wave height and period, but also on their association to spring tide conditions—which is represented by the "resultant height" (*Hr*) variable.

The correlation ratio between environmental parameters and the volumetric/topographic variation was stablished by applying Pearson's Correlation Coefficient (ρ) (Equation 1). ρ interpretation followed the general rule defined by Hinkle, Wiersma, and Jurs (2003), according to which (a) 0.90 to 1.0 indicates very strong correlation; (b) 0.70 to 0.90 indicates strong correlation; (c) 0.50 to 0.70 indicates moderate correlation; (d) 0.30 to 0.50 indicates weak correlation; and (e) 0.0 to 0.30 indicates negligible correlation.

$$\rho = \frac{\sum_{i=1}^{n}(x_i - x)(y_i - y)}{\sqrt{\sum_{i=1}^{n}(x_i - x)^2} \cdot \sqrt{\sum_{i=1}^{n}(y_i - y)^2}} = \frac{\mathrm{cov}(X, Y)}{\sqrt{\mathrm{var}(X) \cdot \mathrm{var}(Y)}} \quad (1)$$

Equation 1 shows Pearson's correlation coefficient definition.

RESULTS

The obtained results are shown below, in terms of atmospheric systems, associated high-energy events, local wave regime, sedimentary volume, and granulometry.

Atmospheric Systems, High-Energy Events, and Local Wave Regime

During the survey period, three high-energy event seasons were described (Table 3 and Figure 3c). These events had an average duration of 8 days, concentrated along the months of January to April of both 2018 and 2019—with the exception of Season 2, which happened in November 2018. Mean response time between storm apexes (minimum atmospheric pressure) and the arrival of the first swell waves was approximately 4 days.

The events with greater intensity reached 4.5 to 5.8 m in maximum resultant height (*Hr*), which refers to the summation of both wave and tide heights (Figure 3c). The coastline of the area was also stricken by a less intense storm surge event in November 2018, with maximum *Hr* of 4.5 m and 4 days of average duration. In all cases, the events were preceded by the development of multiple low atmospheric pressure systems (extratropical cyclones), with average duration of 6 days, between 40°N and 70°N latitude (Figure 4).

An extended analysis of local wave regime showed a clear distinction in terms of significant height (*Hs*) (Figure 3a) and wave type proportion (Figure 3b)—which refers to the percentage of sea and swell waves. The season of smaller waves (0.300.70 m) was distributed between June to October (2017) and May to October (2018). In this scenario, the presence of sea waves started to manifest significantly in June 2017 and May 2018, reaching common predominance in both years (56100%) around July–August.

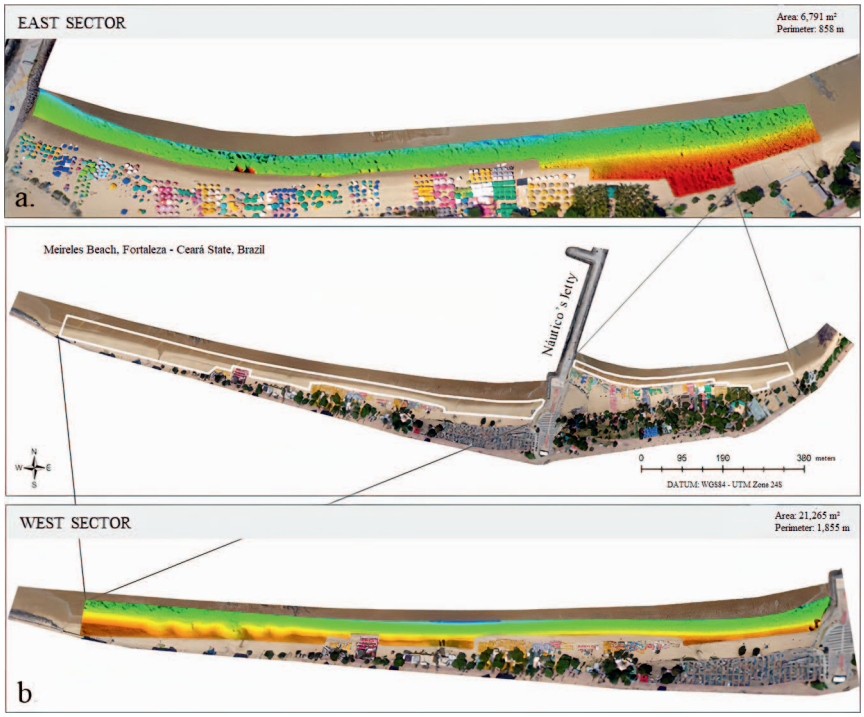

Figure 2. Delimitation of standardized polygons of the (a) east and (b) west sectors.

Bigger waves (0.90–1.20 m) were registered, in general, between December and April—with the exception of 2018, in which a distinct mean *Hs* elevation occurred in November, simultaneously to the second high-energy event season monitored. The predominance (up to 77%) of swell waves with $Hs > 1$ m occurred between February and April.

Sedimentary Volume

The total volume of sand in the area varied as illustrated in Figure 5. Initial rates, which accounted for 63,907 m^3 in volume above custom level (V_{ACL}) and 2.3 m in mean level (ML) in April 2018, suffered a diminution of 25%, resulting in 47,961 m^3 and 2.0 m by the end of May 2018. The greatest volume rate, 74.006 m^3, was recorded in July 2018—after 54.3% relative volume increase—with associated ML of 2.76 m. The value decreases in 14.2% by the end of September 2018, registering $V_{ACL} = 63{,}534$ m^3 and ML = 2.4 m.

Up next, minimum recorded values, 46,430 m^3 (–27%, ML = 1.7 m) in November 2018 and 43,014 m^3 (–7.4%, ML = 1.7 m) in January 2019, were succeeded by a subtle recover of 10.7% in March 2019, reaching $V_{ACL} = 47{,}602$ m^3 and ML = 1.9 m. The final balance reveals a 16,305 m^3 loss (–25.5%) in terms of volume and 0.4 m in terms of mean level (–17.4%) between the first and last survey.

The rate of change of the eastern and western sectors was similar to the overall volumetric change (Figures 5 and 6). However, the east sector ($\Delta V_{ACLmax} = +59.3\%$ and $\Delta V_{ACLmin} = -34.5\%$) showed a tendency for intensification of volumetric changes when compared to the west sector ($\Delta V_{ACLmax} = +53.1\%$ and $\Delta V_{ACLmin} = -25.2\%$). This pattern indicates the dominance of cross-shore sediment transport, as expected for a relatively sheltered coastal area in which the effect of coastal drift is practically nonexistent.

Although quantitative volumetric changes were more significant for the east sector, topographic beach profile modifications became clearer on the west sector (Figure 7). For example, in response to the high-energy events of November 2018, a pronounced beach scarp was formed, mobilizing sand to the lower part of the coast. On the other hand, in the eastern sector this volumetric variation occurs in a way that the movement of

Table 3. *Nomenclature and general information of atmospheric systems development and associated wave response. Dates, Duration (in days) and Minimum Pressure (in hPa), refer to atmospheric systems. Hs_{max}, in meters, refers to maximum significant wave height registered in the study area after cyclonic formation. Response time refers to the interval between storms apexes (minimum atmospheric pressure) and the arrival of the first swell waves.*

	Dates	Duration (days)	Minimum pressure (hPa)	Hs_{max} (m)	Response time
First season (Feb–Apr 2018)	21–28 Feb 2018	7	943	2.63	4
	14–18 Apr 2018	4	951	1.78	3
Second season (Nov 2018)	13–17 Nov 2018	5	953	2.32	3
Third season (Feb 2019)	03–10 Feb 2019	7	960	1.75	4
	20–26 Feb 2019	6	937	1.54	4

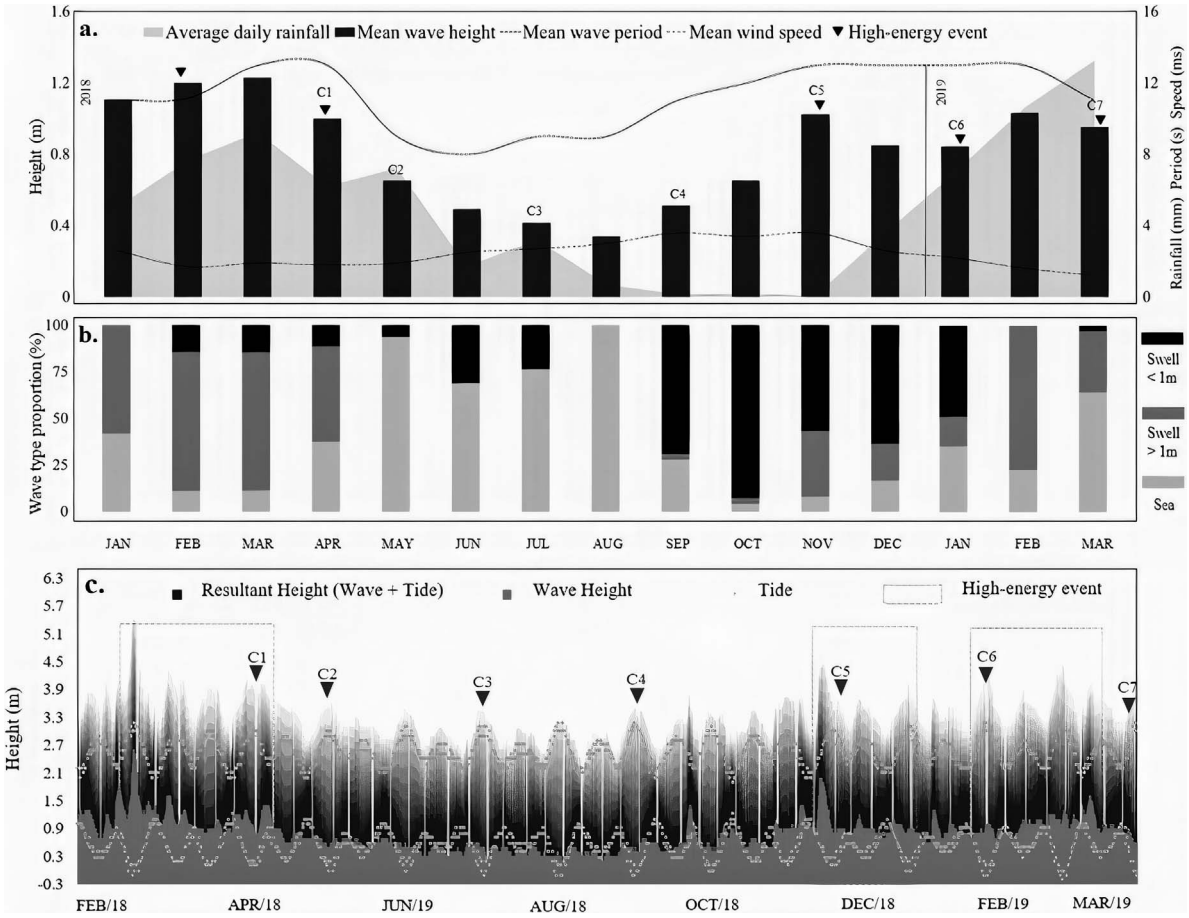

Figure 3. Monthly characterization of (a) environmental variables, (b) wave type proportion and distribution of tides, significant wave height (*Hs*), and resultant wave height (*Hr*) for the (c) survey period, with high-energy season's and survey date delimitation.

sediments does not cause great morphological variations in the beach profile.

Granulometry

The analysis of 78 sampling points along the foreshore (FS) and backshore (BS) sectors revealed a faciologic composition slightly variable from fine to medium lithoclastic sand, mainly well sorted (Table 4). On the backshore zone, throughout the survey period, there was a predominance of medium sand in proportions of 57% to 89%. The foreshore zone, however, experienced more expressive variations between fine sand (14 to 75%) and medium sand (25% to 86%), especially from September to November 2018.

The kurtosis parameter (K_G) was predominantly mesokurtic for both sectors, with punctual expression of platykurtic patterns for the samples collected in surveys C4 and C7, for foreshore and backshore sectors, respectively.

Greater discrepancies in granulometric parameters were observed between September and November 2018, revealing the abrupt change potential of the second high-energy event. An inversion of granulometric classification occurred on the foreshore as medium sand replaced fine sand facies previously predominant (75%), in an 86% proportion. Selection degree (σ), previously 92% well selected, showed a relevant moderate selection sediments insertion (43%), with an accentuation of the symmetry of the Gaussian curve (42% to 86%) and transition from platykurtic to mesokurtic character. A similar variation pattern was noted on the backshore for each of the parameters, however with a subtle numeric discrepancy (Table 4).

In relation to east and west sector, a distinction between facies was noted—which was disturbed, more significantly, by the events prior to the C5 survey (Table 5). On the east sector, under lower energy conditions established by the presence of rocky outcrops and the influence of Mucuripe Harbor, well-selected fine sand was predominant, with approximately symmetric and meso/leptokurtic Gaussian curves. On the west sector, well-selected medium sand facies predominated (except in C7), with approximately symmetric mesokurtic curves. In both sectors, a variation pattern compatible with that observed in Table 4 was expressed—showing similar response behaviors for the whole system of the survey area.

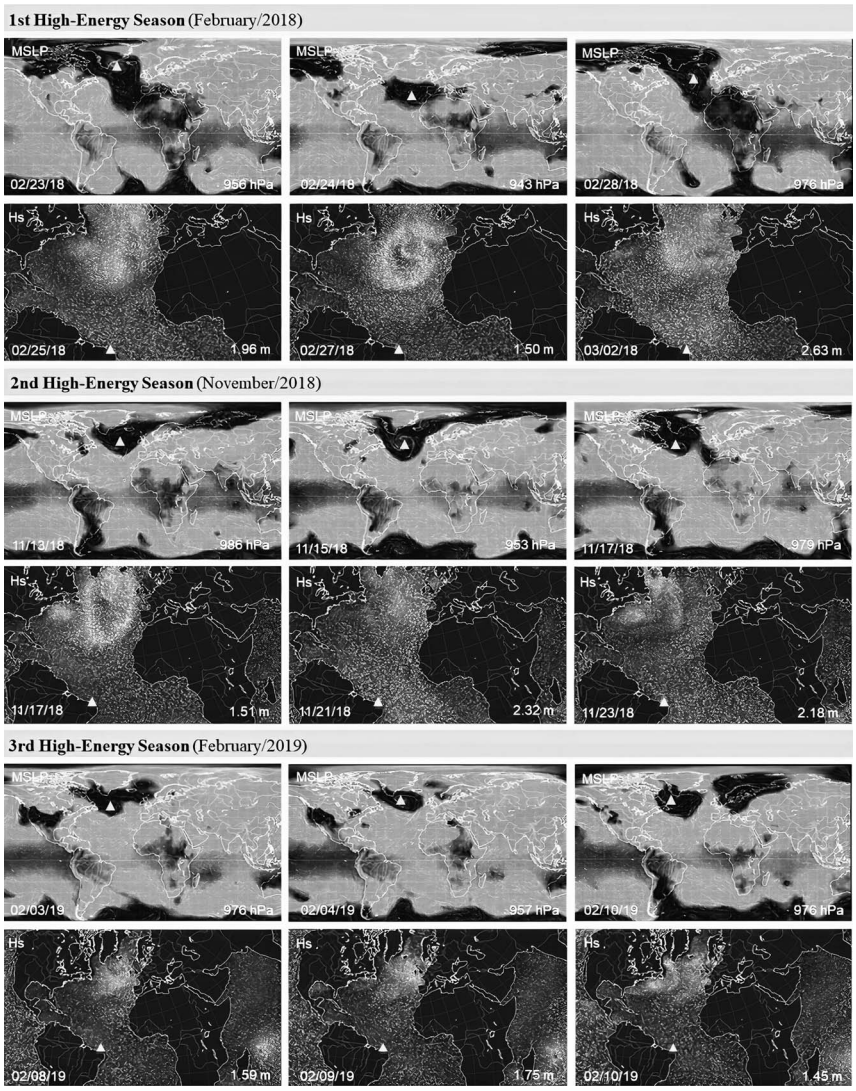

Figure 4. Mean sea level pressure (MSLP) and significant wave height (*Hs*) imagery, showing the development of atmospheric systems in North Atlantic and associated swell wave's arrival on the Northeastern Brazilian coast. A triangle marks the measurement sites in representative high-energy events of each season.

Interaction of Variables

The set of data illustrated in Figure 6 correlates numerically as indicated in Table 6. Total sedimentary volume (V_{ACL}) and mean level (ML) presented a moderate-to-strong correlation with incident wave type, in the proportions of ±0.638 and ±0.775, respectively. As a result, wave period (*T*) correlated moderately at a rate of –0.504 with V_{ACL} and –0.625 with ML. Significant wave height (*Hs*) and resultant wave height (*Hr*) had negligible and moderate correlation, respectively. The least significant connections of V_{ACL} and ML were correlated to mean wave speed (Wspd), in proportions of 0.025 and –0.061.

DISCUSSION

Beach face erosion and recovery phases often occur in cyclic events concomitant to seasonal climatic variations, delimitating characteristic volumetric profiles for summer and winter seasons (Clarke and Eliot, 1983; Owens, 1977; Schwartz, 1967; Shepard, 1950; Short, 1980). At the study site, sedimentary balance over a 1-year period presented a cyclic variation tendency, moderately correlated to local wave climate, in which the atmospheric climatology of the Northern Hemisphere plays an important role.

The period of significant volumetric accretion was related to mild weather environmental conditions, especially in terms of wave period and height. Lower volumetric values were recorded during the predominance of swell waves smaller than 1 m and in periods of greater wave type variability; a similar response to the one described by Dubois (1988) in Delaware, USA. Total sedimentary balance resulted in an erosive tendency of about 25.5% of the beach profile. This rate might illustrate a representative and recurrent behavior of the area,

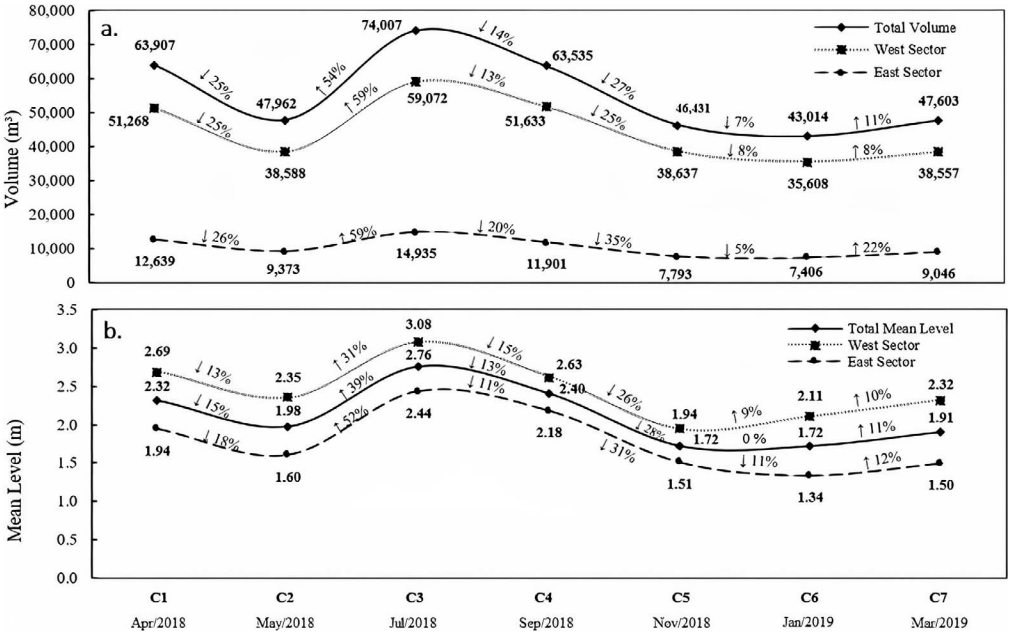

Figure 5. (a) Volume above custom level (V_{ACL}) curves and (b) mean level (ML) curves, with associated variation rate for the entire area and its sectors, through each survey interval.

considering its history of anthropic interventions aiming to prevent such phenomenon.

Despite cyclic variation, the distinction between summer and winter topography, as synthetically established by Bruun's Rule (Bruun, 1962), for instance, must be applied with caution when considering the effect of swell waves. In two out of the three monitored cases, the occurrence of multiple storm surge events was related to positive volumetric changes within its bimonthly period of incidence on the coast. Similar processes were described by Dail, Merrifield, and Bevis (2000) and Dubois (1988) on sandy beaches in Delaware and Hawaii, in which storm wave incidence caused immediate berm erosion, followed by a quick process of vertical—and later on, horizontal—accretion on the beach face. In addition, other authors highlight the effect of milder swell waves, subsequent to high-energy events, on the reconstruction of beach profile topography (Quartel, Kroon, and Ruessink, 2008; Shepard, 1950).

Furthermore, it is important to highlight the role of local morphodynamics on sedimentary balance based on the distinct responses of both sectors. Modification patterns of the east sector, for instance, with softer geomorphological variations in response to sediment movement, can be explained considering the presence of the jetty and rocky outcrops and their role in sediment retention, which characterizes a relatively more

Table 4. *Percentage distribution of granulometric parameter classification on foreshore (FS) and backshore (BS) sectors.*

	C3 (%)		C4 (%)		C5 (%)		C6 (%)		C7 (%)	
	FS	BS	FS	BS	FS	BS	FS	BS	FS	BS
Folk and Ward (1957)										
Medium sand	33	57	25	83	86	89	67	83	50	67
Fine sand	67	43	75	17	14	11	33	17	50	33
Selection degree (σ)										
Good selection	92	86	92	83	57	56	100	50	88	100
Moderate selection	8	14	8	17	43	44	—	50	13	—
Symmetry (S_{ki})										
Approx. symmetric	67	43	42	33	86	89	100	83	86	50
Positive symmetry	33	29	16	33	—	—	—	—	14	50
Negative symmetry	—	29	42	33	14	11	—	17	—	—
Kurtosis (K_G)										
Mesokurtic	33	57	25	50	86	78	50	50	57	17
Platykurtic	33	29	42	33	14	11	17	33	29	66
Leptokurtic	25	—	33	17	—	11	33	17	14	17
Very leptokurtic	8	14	—	—	—	—	—	—	—	—

Table 5. *Percentage distribution of granulometric parameter classification on east (ES) and west (WS) sectors.*

	C3 (%)		C4 (%)		C5 (%)		C6 (%)		C7 (%)	
	ES	WS	ES	WS	ES	WS	ES	WS	ES	WS
Folk and Ward										
Medium sand	—	57	17	58	50	100	25	100	—	73
Fine sand	100	43	83	42	50	—	75	—	100	27
Selection degree (σ)										
Good selection	100	86	100	75	25	50	100	62	100	9
Moderate selection	—	14	—	25	75	50	—	38	—	91
Symmetry (S_{ki})										
Approx. symmetric	40	64	66	25	100	83	75	100	50	73
Positive symmetry	40	29	17	25	—	—	—	—	50	27
Negative symmetry	20	7	17	50	—	17	25	—	—	—
Kurtosis (K_G)										
Mesokurtic	—	58	66	8	100	75	—	75	—	45
Platikurtic	40	21	17	50	—	17	25	25	—	55
Leptokurtic	—	21	17	42	—	8	75	—	100	—
Very leptokurtic	60	—	—	—	—	—	—	—	—	—

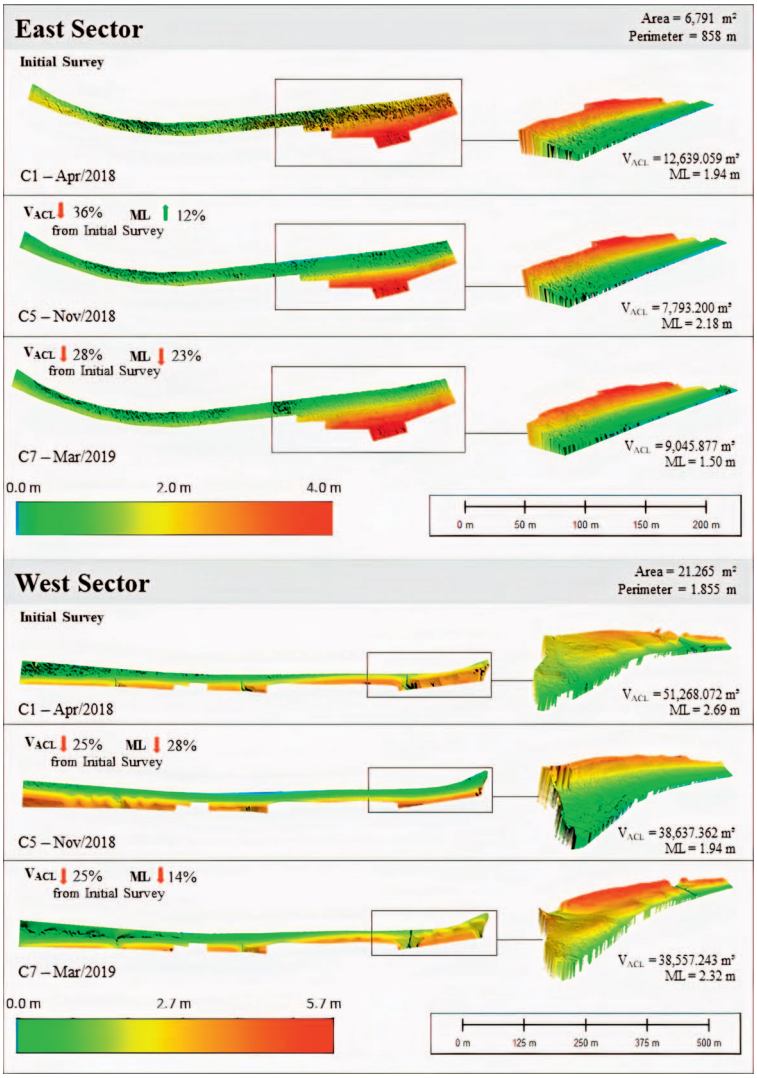

Figure 6. Digital elevation models (DEMs) of East and West sectors on missions C1 (first survey), C5 (greater beach profile variability survey), and C7 (final survey), highlighting areas with notable topographic profile changes.

sheltered zone than the west sector. Intense anthropic interference and a high degree of artificialization in coastal areas establish morphodynamic conditions in which the application of synthesized models, such as that of Bruun, become particularly limited (Cooper and Pilkey, 2004). To reach this conclusion, sedimentological characterization was a key aspect, reinforcing different patterns of energetic conditions and their variation in response to rapid forcing of high-energy waves, similar to the findings of Herrling and Winter (2014) and Miot da Silva, Mousavi, and Jose (2012).

Regarding correlations between environmental variables, sedimentary balance variations showed a predominant connection to wave–tide conditions. In general, all wave parameters presented moderate-to-strong relation to beach volume and mean level. However, an exception to this tendency was found in significant height (*Hs*), showing that wave height alone does not cause relevant variations in volume and level—but its association with spring tide does have considerable effects.

In the multi-methodological approach, huge advantages were noted in using an association of direct and indirect methods. The UAV-based photogrammetric tool was confirmed to be very effective, especially in terms of accuracy and cost–benefit relation in the function of survey area cover and logistics, as previously highlighted in many current studies (Brunier *et al.*, 2016; Casella *et al.*, 2014; Cheng, Wang, and Guo, 2016; Gonçalves and Henriques, 2015; Papakonstantinou, Topouzelis, and Pavlogeorgatos, 2016; Yoo and Oh, 2016). However, the association of this tool with *in situ* and satellite derived data allowed better understanding of the variables and processes involved in sedimentary budget.

Although this study provides a valuable perspective over local and possible regional patterns of sedimentary balance, the need for further elucidation of the submerged sector with

Figure 7. Visual topographic profile changes in two distinct portions of the West Sector during (a and c) C2, May 2018 and (b and d) C5, Nov 2018.

bathymetric surveys (Hallermeier, 1981), in order to fully understand sedimentary motion within the entire coastal system, is recognized.

CONCLUSIONS

Under the influence of Northeast Brazil's characteristic environmental conditions, the sedimentary balance of Fortaleza's foreshore and backshore is mainly affected by local wave regime variations. In this scenario, a strong correlation was identified between extratropical cyclone formation on the Northern Hemisphere and the incidence of high-energy waves on the northeastern Brazilian coast, with a mean response time of 4 days between apexes of mean sea level pressure (hPa) and *Hs* (m).

Local wave regimes presented a clear distinction throughout the year in terms of *Hs* (m) and *T* (s), in phase with factors of climatic seasonality and interhemispheric connection. The season of high-energy waves concentrated on the first semester, from January to April, with greater incidence of amplified swell waves and occurrence of more intense storm surges. Between May and August, the predominance of sea waves and the action of characteristically strong winds revealed a decrease of interhemispheric connection influence, associated with maximum sedimentary accumulation rates.

The erosive tendency of the area during the survey period, represented by a sedimentary balance of 25.5% volumetric decrease, was mostly related to environmental conditions marked by longer wave periods and greater wave type variability. The immediate effect of storm surges in this context, despite the remarkable potential for abrupt modifications on local volumetric profile and granulometry, still requires more detailed elucidation—especially concerning the role of less intense swell waves in beach profile reconstruction.

Subtle granulometric variations indicate that the area is, most of the time, under a relative energetic balance. Disturbances in this system occur more intensively on the medium portion of superior backshore, highlighting the importance of monitoring this sector due to its relevance in the sedimentary mobilization process.

Table 6. *Pearson's correlation coefficient (ρ) for significant height (*Hs*), resultant height (*Hr*), wave period (*T*), mean wind speed (Wspd), precipitation (Prec), total volume (V_{ACL}), mean level (ML), sea wave proportion (%sea) and swell wave proportion (%swell).*

	Hs (m)	*Hr* (m)	*T* (s)	Wspd (m/s)	Prec (mm)	V_{ACL} (m^3)	ML (m)	% sea	% swell
Hs (m)	1	0.875	0.764	−0.840	0.940	**−0.239**	**−0.256**	−0.509	0.509
Hr (m)		1	0.893	−0.615	0.744	**−0.460**	**−0.516**	−0.745	0.745
T (s)			1	−0.319	0.568	**−0.504**	**−0.625**	−0.935	0.935
Wspd (m/s)				1	−0.930	**0.025**	**−0.061**	0.001	−0.001
Prec (mm)					1	**−0.292**	**−0.239**	−0.302	0.302
V_{ACL} (m^3)						**1**	**0.977**	**0.638**	**−0.638**
ML (m)							**1**	**0.775**	**−0.775**
% sea								1	−1
% swell									1

Correlation analysis showed that sedimentary variation occurs mainly as a function of wave–tide conditions. While wave period—and, consequently, its type—has strong influence, wave height alone does not follow the same tendency, which highlights the role of associated tide conditions.

To attend this objective and the general aim of this study, the application of direct and indirect methods was undoubtedly advantageous—highlighting changes in both large and local scale, in different chronological series.

ACKNOWLEDGMENTS

The study was supported by the project "Study of coastal dynamics using a drone in 3D imaging associated with detailed monitoring of climatic variables—PIBIC UFC." Moreover, we thank CNPq for the Research Productivity Fellowship (CNPq 309140/2018-8, Pinheiro, L.), and FUNCAP for the DCR Fellowship (Claudino-Sales, V.) and Science Initiation scholarship (Eduardo, L.M.).

LITERATURE CITED

Alves, J.H.G.M., 2006. Numerical modeling of ocean swell contributions to the global wind-wave climate. *Ocean Modelling*, 11, 98–122.

Barrer, N.F. and Ursell, F., 1948. The generation and propagation of ocean waves and swell—I. Wave periods and velocities. *Philosophical Transactions of the Royal Society of London, Series A. Mathematical and Physical Sciences*, 240(824), 527–560.

Bezerra, M.O.; Pinheiro, L.; and Morais, J.O., 2007. Shoreline Change of the Mucuripe Harbour Zones (Fortaleza-Ceará, Northeast Brazil) 1972–2003. *In:* Lemckert, C. (ed.), *ICS 2007 Proceedings (Gold Coast, Queensland, Australia) Journal of Coastal Research*, Special Issue No. 50, pp. 1163–1167.

Brunier, G.; Fleury, J.; Anthony, E.J.; Gardel, A. and Dussouillez, P., 2016. Close-range airborne Structure-from-Motion Photogrammetry for high-resolution beach morphometric surveys: Examples from an embayed rotating beach. *Geomorphology*, 261, 76–88.

Bruun, P., 1962. Sea level rise as a cause of shore erosion. *Proceedings of the American Society of Civil Engineers, Journal of Waterways and Harbors Division*, 88, 117–130.

Camargo, M.G., 2006. Sysgran: um sistema de código aberto para análise granulométrica do sedimento. *Revista Brasileira de Geociências*, 36(2), 371–378.

Carvalho, A.M., 2003. Dinâmica costeira entre Cumbuco e Matões-Costa NW do Estado do Ceará. Ênfase nos processos eólicos. Salvador, Brazil: Universidade Federal da Bahia, UFBA, Ph.D. dissertation, 188p.

Casella, E.; Rovere, A.; Pedroncini, A.; Mucerino, L.; Casella, M.; Cusati, L.A.; Vacchi, M.; Ferrari, M., and Firpo, M., 2014. Study of wave run up using numerical models and low-altitude aerial photogrammetry: A tool for coastal management. *Estuarine, Coastal and Shelf Science*, 149, 160–167.

Chen, G.; Chapron, B.; Ezraty, R., and Vandemark, D., 2002. A global view of swell and wind sea climate in the ocean by satellite altimeter and scatterometer. *American Meteorological Society*, 19, 1849–1859.

Cheng, J.; Wang, P., and Guo, Q., 2016. Measuring beach profiles along a low-wave energy microtidal coast, west-central Florida, USA. *Geosciences*, 6(4), 44.

Chung, J.C., 1982. Correlations between the tropical Atlantic trade winds and precipitation in northeastern Brazil. *Journal of Climatology*, 2(1), 35–46.

Clarke, D.J. and Eliot, I.G., 1983. Mean sea-level and beach-width variation at Scarborough, Western Australia. *Marine Geology*, 51, 251–267.

Claudino-Sales, V., 1993. Cenários litorâneos—Lagoa do Papicu, natureza e ambiente na cidade de Fortaleza, Ceará. São Paulo, Brazil: Universidade Federal de São Paulo, USP, Master's thesis, 349p.

Claudino-Sales, V.; Wang. P., and Carvalho, A.M., 2018. Interactions between various headlands, beaches and dunes along the coast of Ceara State, Northeast Brazil. *Journal of Coastal Research*, 34(2), 413–428.

Cooper, J.A.G. and Pilkey, O.H., 2004. Sea level rise and shoreline retreat: Time to abandon the Bruun Rule. *Global and Planetary Change*, 43, 157–171.

Dail, H.J.; Merrifield, M.A., and Bevis, M., 2000. Steep beach morphology changes due to energetic wave forcing. *Marine Geology*, 162, 443–458.

DNH. 2021. Centro de Hidrografia da Marinha. *Tábuas de Maré*. https://www.marinha.mil.br/chm/tabuas-de-mare

Drennan, W.M.; Graber, H.C.; Hauser, D., and Quentin, C., 2003. On the wave age dependence of wind stress over pure wind seas. *Journal of Geophysical Research*, 30, 1–13.

Dubois, R.N., 1988. Seasonal changes in beach topography and beach volume in Delaware. *Marine Geology*, 81, 79–96.

Farias, E.G.G., 2012. Uso de dados obtidos por sensores orbitais ativos no estudo dos campos de ondas de superfície no Atlântico Norte Tropical. São José dos Campos, Brazil: Instituto Nacional de Pesquisas Espaciais (INPE), Pós-Graduação em Sensoriamento Remoto, Ph.D dissertation, 207p.

Fechine, J.A.L., 2007. Alterações no perfil natural da zona costeira da cidade de Fortaleza, Ceará, ao longo do século XX. Fortaleza, Brazil: Universidade Federal do Ceará, Master's thesis, 116p.

Fisch, C.L., 2008. Caracterização do Clima de Ondas na Costa do Ceará. Rio de Janeiro, Brazil: Universidade Federal do Rio de Janeiro, Master's thesis, 231p.

Folk, R.L. and Ward, W.C., 1957. Brazos River bar: A study in the significance of grain size parameters. *Journal of Sedimentary Petrology*, 27, 3–26.

GFS. 2020. National Centers for Environmental Information. *Global Forecast System (GFS)*. https://www.ncdc.noaa.gov/data-access/model-data/model-datasets/global-forcast-system-gfs

Gonçalves, J.A. and Henriques, R., 2015. UAV photogrammetry for topographic monitoring of coastal áreas. *ISPRS Journal of Photogrammetry and Remote Sensing*, 104, 101–111.

Guerra, R.G.P., 2014. Vulnerabilidade costeira a eventos de alta energia no Litoral de Fortaleza, Ceará. Fortaleza, Ceará, Brazil: Universidade Federal do Ceará, Programa de Pós-Graduação em Ciências Marinhas Tropicais, Master's thesis, 103p.

Hallermeier, R.J., 1981. A profile zonation for seasonal sand beaches from wave climate. *Coastal Engineering*, 4, 253–257.

Hamilton, G.D., 1992. Measurements of long-period, low-amplitude swell in the western North Atlantic. *American Meteorological Society*, 9, 645–658.

Herrling, G. and Winter, C., 2014. Morphological and sedimentological response of a mixed-energy barrier island tidal inlet to storm and fair-weather conditions. *Earth Surface Dynamics*, 2, 363–382.

Hinkle, D.E.; Wiersma, W., and Jurs, S.G., 2003. *Applied Statistics for the Behavioral Sciences*, 5th edition. Boston: Houghton Mifflin, 756p.

INMET, 2020. INMET—*BDMEP* (Banco de Dados Meteorológicos do Instituto de Nacional de Meteorologia) https://bdmep.inmet.gov.br/

Innocentini, V.; Cunha Prado, S.C.S.; Pereira, C.S.; Arantes, F.O., and Brandão, I.N., 2000. Marulhos no litoral norte do Brasil gerados por furacões: Caso de 24 de outubro de 1999. *Revista Brasileira de Meteorologia*, 16(2), 177–186.

IPECE, 2018. Perfil Municipal 2017. Instituto de Pesquisa e Estratégia Econômica do Ceará IPECE. Fortaleza. Ano I–janeiro de 2018.

Köppen, W., 1936. Das geographische System der Klimate. *In*: Köppen, W. and Geiger, R. (eds.), *Handbuch der Klimatologie*, Volume I, Part C. Berlin: Gerbrüder Borntraeger, 44p.

Lima Filho, R.P.; Castelo Branco, M.P.N., and Pinheiro, L.S., 2019. Contribuição do rio Cocó e riacho Maceió na sedimentação da plataforma interna de Fortaleza-CE. *REGNE*, 5., 137–149.

Maia, L.P., 1998. Procesos costeros y balance sedimentario a lo largo de Fortaleza (NE-Brasil): implicaciones para una gestión adecuada

de la zona litoral. Barcelona: Universitat de Barcelona, Ph.D. dissertation.

Maia, L.P.; Jimenez, J.A.; Serra, J., and Morais, J.O., 1998. The coastline of Fortaleza City. A product of environmental impacts caused by the Mucuripe Harbor. *Arquivos de Ciências do Mar*, 31, 93–100.

Maia, L.P.; Jimenez, J.A.; Serra, J.; Morais, J.O., and Sanchez-Arcilla, A., 1996. The Fortaleza (NE Brazil) Waterfront: Port versus Coastal Management. *Journal of Coastal Research*, 14(4), 1284–1292.

Mendes, D. and Mendes, M.D., 2004. Climatology of cyclones, anticyclones and storm tracks: Revision of concepts. *Revista Brasileira de Geofísica*, 22(2), 127–134.

Miot da Silva, G.; Mousavi, S.M.S., and Jose, F., 2012. Wave-driven sediment transport and beach-dune dynamics in a headland bay beach. *Marine Geology*, 323–325, p.29–46.

Morais, J.O., 1980. Aspectos do transporte de sedimentos no litoral do município de Fortaleza, Estado do Ceará, Brasil. *Arquivos de Ciências do* Mar, 20(1), 71–100.

Morais, J.O., 1981. Evolução sedimentológica da enseada de Mucuripe (FortalezaCeará – Brasil). *Arquivos de Ciências do Mar*, 21(1), 19–46.

Morais, J.O.; Pinheiro, L.; Pessoa, P.R.S.; Freire, G.S.; Carvalho, A.M.; Guerra, R.G.P.; Barros, E.L., and Moura, F.J.M., 2018. Ceará. *In:* Dieter Muehe. (Org.). *Panorama da Erosão Costeira no Brasil*. Volume 1, 1st edition. Brasília: MMA, pp. 261–289.

Moura, M.R., 2012. Dinâmica costeira e vulnerabilidade à erosão do litoral dos municípios de Caucaia e Aquiraz, Ceará. Fortaleza, Brazil: Universidade Federal do Ceará, Master's thesis, 210p.

Munk, W.H.; Miller, G.R.; Snodgrass, F.E., and Barber, N.F., 1963. Directional recording of swell from distant storms. *Philosophical Transactions of the Royal Society A*, 255, 505–584.

Owens, E.H., 1977. Temporal variations in beach and nearshore dynamics. *Journal of Sedimentary Petrology*, 47, 168–190.

Papakonstantinou, A.; Topouzelis, K., and Pavlogeorgatos, G., 2016. Coastline zones identification and 3D coastal mapping using UAV spatial data. *International Journal of Geo-Information*, 5(75).

Paula, D.P.; Morais, J.O.; Ferreira, O., and Dias, J., 2015a. Análise histórica das ressacas do mar no litoral de Fortaleza (Ceará, Brasil): origem, características e impactos. *Ressacas do Mar, Temporais e Gestão Costeira*. Fortaleza, Brazil: Editora Premius, pp. 173–201.

Paula, D.P.; Morais, J.O.; Ferreira, O., and Dias, J., 2015b. De um simples porto a uma cidade convertida para o turismo: artificialização do litoral de Fortaleza-CE, Brasil. *O Homem e as Zonas Costeiras*, Tomo IV. Rio de Janeiro, Brazil: Rede BrasPor, Faperj.

Pinheiro, L.S.; Coriolano, L.N.; Costa, M.F., and Dias, J.A., 2008. O Nordeste Brasileiro e a Gestão Costeira. *Revista de Gestão Costeira Integrada*, 8(2), 5–10.

Pinheiro, L.S.; Morais, J.O., and Maia, L.P., 2016. The beaches of Ceará. *In:* Short, A.D. and Henrique da F. Klein, A. (eds.), *Brazilian Beaches System*. Coastal Research Library. Volume 1, 1st edition: Springer International Publishing, pp. 175–199.

PNBOIA, 2021. Centro de Hidrografia da Marinha. *Dados PNBOIA*. https://www.marinha.mil.br/chm/dados-do-goos-brasil/pnboia-mapa

Quartel, S.; Kroon, A., and Ruessink, B.G., 2008. Seasonal accretion and erosion patterns of a microtidal sandy beach. *Marine Geology*, 250, 19–33.

Schwartz, M.L., 1967. The Bruun theory of sea-level rise as a cause of shore erosion. *The Journal of Geology*, 75(1), 76–92.

Semedo, A.; Suselj, K.; Rutgersson, A., and Sterl, A., 2011. A global view on the wind sea and swell climate and variability from ERA-40. *American Meteorological Society*, 24, 1461–1479.

Shepard, F.P., 1950. Beach cycles in southern California. *United States Beach Erosion Board*, Tech. Memo. No. 20, 26p.

Short, A.D., 1980. Beach response to variations in breaker height. *Proceedings of Coastal Engineering Conference* (Sydney, Australia, 7th American Society of Civil Engineers), pp. 1016–1035.

Silva, A.C.; Facanha, P.; Bezerra, C.; Araujo, A., and Pitombeiras, E., 2011. Características das ondas "sea" e "swell" observadas no litoral do Ceará-Brasil: variabilidade anual e inter-anual. *Tropical Oceanography*, 39(2), 123–132. Recife.

Suguio, K., 1973. *Introdução a Sedimentologia*. São Paulo, Brazil: Edgard Blucher/EDUSP, 317p.

Trigo, I.F.; Davies, T.D., and Bigg, G.R., 1999. Objective climatology of cyclones in the Mediterranean region. *Journal of Climate*, 12, 1685–1696.

Utida, G.; Cruz, F.W.; Etourneau, J.; Bouloubassi, I.; Schefub, E.; Vuille, M.; Novello, V.F.; Prado, L.F.; Sifeddine, A.; Klein, V.; Zular, A.; Viana, J.C.C., and Turcq, B., 2019. Tropical South Atlantic influence on Northeastern Brazil precipitation and ITCZ displacement during the past 2300 years. *Scientific Reports*, 9(1), 1698.

Vassie, J.M.; Woodworth, P.L., and Holt, M.W., 2004. An example of North Atlantic deep-ocean swell impacting ascension and St. Helena Islands in the central South Atlantic. *American Meteorological Society*, 21, 1095–1103.

Vianna, M.L., 2000. Ressacas na costa norte do nordeste causadas por furacões extratropicais. In: IX Congresso Brasileiro de Meteorologia. Rio de Janeiro-RJ, pp. 2613–2619.

Wentworth, C.K., 1922. A scale of grade and class terms for clastic sediments. *The Journal of Geology*, 30(5), 377–392.

Yoo, C.I. and Oh, T.S., 2016. Beach volume change using UAV photogrammetry in Songjung Beach, Korea. *The International Archives of the Photogrammetry, Remote Sensing and Spatial Information Sciences—XXIII ISPRS Congress*, XLI-B8, 1201–1205.